Analysis of micro-Fresnel lenses with local grating theory and its comparison with fully electromagnetic methods

Hiroyuki Ichikawa,[1,*] Koji Masuda,[2] and Takeshi Ueda[2]

[1]*Faculty of Engineering, Ehime University, Matsuyama 790-8577, Japan*
[2]*Imaging Engine Development Division, Ricoh, Ebina 243-0460, Japan*
[*]*Corresponding author: hichikaw@dpc.ehime-u.ac.jp*

Received May 20, 2009; revised July 15, 2009; accepted July 17, 2009;
posted July 22, 2009 (Doc. ID 111435); published August 13, 2009

We report on a numerical analysis method for diffractive optical elements that consist of features ranging from subwavelength to more than 10λ. The essence of the method is treating local structures of the optical elements as diffraction gratings. It is shown that the method can provide accuracy of results comparable with fully electromagnetic treatments in much shorter time. The theory and results are explained assuming micro-Fresnel lenses with one-dimensional structures for investigating polarization properties. © 2009 Optical Society of America

OCIS codes: 050.1755, 050.1950, 050.1965, 050.1970, 260.2110.

1. INTRODUCTION

Numerical tools for designing and analyzing diffractive optical elements (DOEs) depend on diffraction domains determined by the feature sizes compared with the wavelength [1]. Perhaps the most widely used DOEs in a variety of applications would have feature sizes between λ and several tens of λ, λ being the wavelength of light in vacuum, but analyzing such DOEs is not so easy [2]. Inclusion of small features makes full scalar theory less accurate, while full vector theory is too heavy to implement. Therefore, some sort of hybrid approach should provide comfortable computation speed with acceptable accuracy. Several approaches have been reported for challenging this problem [3–5].

For this purpose, we propose to use a method in which a local structure of an optical element is assumed as an infinitely extending diffraction grating. We refer to it as local grating theory (LGT). This concept was mentioned in the literature as early as 1962 [6]. In terms of diffractive optics, perhaps Noponen *et al.* first explicitly stated "a diffractive lens may be viewed locally as such a grating" [7], p. 437. Their purpose for this approach was to improve diffraction efficiency of diffractive lenses in the resonance domain, and such gratings were expected to behave as prisms. Sheng *et al.* expanded the method for optimizing two-dimensional circular diffractive lenses [8], and Kleemann and Güther conducted further detailed study [9].

In this paper, we apply a LGT whose basic concept is similar to those of [8,9]—but in a form easier to implement—to one-dimensional micro-fresnel lenses.

There are two reasons for using simpler one-dimensional structures rather than more practical and useful two-dimensional ones. First, we need to know the accuracy and applicability of the LGT by comparing results with those of other well-established numerical methods, such as the Fourier modal method (FMM) [10] and the finite-difference time-domain (FDTD) method [11], in addition to experimental data. Second, we would like to investigate the polarization-handling ability of the LGT, for which experiments with one-dimensional structures are ideal.

2. PRINCIPLE

As the term local grating theory indicates, the local structure of a DOE with a wide variety of feature sizes is assumed as a diffraction grating. For example, in the case of a micro-Fresnel lens, each zone is assumed to behave as if it were a one-dimensional grating of infinite extent, and the function of the entire lens is obtained by summing up the effect of each zone. An analyzed optical system is shown in Fig. 1. Diffractive surface relief structure is created at the boundary of two half-spaces with refractive indices n_1 and n_2. A plane wave normally illuminates a micro-Fresnel lens whose surface relief depth, focal length, and radius are h, f, and r, respectively. Propagation through the surface relief diffractive structure is analyzed by any electromagnetic diffraction grating theory, but in an approximate way. We employ the FMM because of its widely accepted accuracy and computation speed in addition to relative simplicity for implementation.

A. Complex Amplitude

First of all, the phase profile of a micro-Fresnel lens of L phase levels is

$$\phi(x) = l\Phi, \quad \text{for } -(l+1)\Phi < \mathrm{mod}[\phi_0(x), 2\pi] \leqslant -l\Phi, \tag{1}$$

where

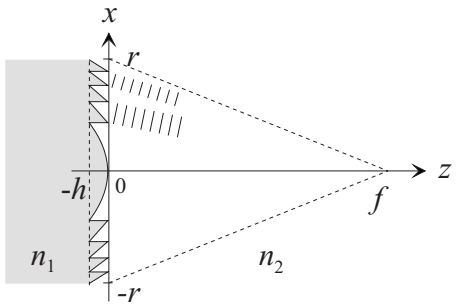

Fig. 1. Analyzed optical system. Surface relief layer $-h \leq z \leq 0$ is analyzed by an electromagnetic diffraction grating theory.

$$\phi_0(x) = 2\pi n_2(f - \sqrt{f^2 + x^2})\lambda \tag{2}$$

is a phase profile of an aberration-free lens, $0 \leq l \leq L-1$, $\Phi = -2\pi/L$, and mod(p,q) denotes the remainder of an operation p/q. In this way, a position x and a discrete phase at the location are related. Now, the number of zones corresponding to a 2π phase is given by

$$M_L = \text{int}[(\sqrt{f^2 + r^2} - f)\lambda] + 1, \tag{3}$$

where r is a diameter of the lens and int(q) denotes the maximum integer that is not larger than q.

We place equally spaced sampling points at $x = x(n) = n\Delta x$—where $\Delta x = 2r/N$ and n is an integer of $|n| \leq N/2$—for evaluating complex amplitudes, and the values of them at the exit plane of the micro-Fresnel lens are computed with the FMM (see Fig. 2). In applying a fast Fourier transform (FFT) algorithm, n must be a power of 2 and a sampling point numbered $n = 0$ must be at $x = 0$. Then, the two points $x = r$ and $-r$ are equivalent.

The locations of an outer boundary of an mth subzone of equiphase is

$$x_m = \sqrt{m^2\lambda^2 + 2mLf\lambda}L. \tag{4}$$

Note that the outermost zone and subzone are limited by the lens radius, of course.

At sampling point $x(n)$, the lens is assumed to behave as an L-level phase grating with period of

$$d(n) = x_{P+L} - x_P, \tag{5}$$

where $x_{m-1} < x(n) \leq x_m$ and $P = \text{int}[(m-1)/L]L$. The grating depth at $x(n)$ is then

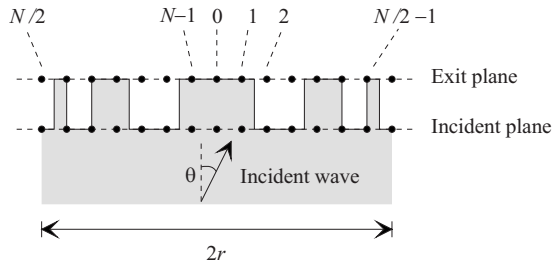

Fig. 2. Location of sampling points and their numbering order in the surface relief layer of a micro-Fresnel lens, for example. θ is an incidence angle.

$$h(n) = \frac{\lambda}{|n_2 - n_1|}\left(\text{int}\left[\frac{m-1}{L}\right] - \frac{m}{L} + 1\right). \tag{6}$$

For example, in the case of $L = 4$ (Fig. 3), the period is $x_8 - x_4$ and the depth is h' at the sampling point of $x(n)$. Here

$$h' = \lambda/L|n_2 - n_1| \tag{7}$$

is the depth corresponding to a single phase step.

Complex amplitude $u(n,0)$ at $x = x(n)$ and $z = 0$ is given by the FMM assuming that the jth zone is treated as a grating of period $d_j = x_{jL} - x_{(j-1)L}$ (Fig. 4) with the representation

$$u(n,0) = \sum_q T_q \exp(i\alpha_q \bar{x}), \tag{8}$$

where T_q is the complex amplitude of a transmitted plane wave of qth order, $\alpha_q = 2\pi(n_1 \sin\theta/\lambda + q/d_j)$, and $\bar{x}$ is the distance from the inner boundary of the zone to $x(n)$. Then, even if two sampling points are located in the same subzone, different complex amplitude values are assigned. Applying the FMM here, the effects of reflection can be included in evaluating optical power in the focal plane.

In addition, it is convenient to convert $u(n,0)$ in Eq. (8) in the following way:

$$u(n,0) \leftarrow \begin{cases} u(n,0)\sqrt{n_2/n_1}, & \text{for TE} \\ u(n,0)\sqrt{n_1/n_2}, & \text{for TM} \end{cases}. \tag{9}$$

This enables direct comparison of finally obtained intensity profiles between TE and TM polarization at the end of the simulation.

B. Propagation from the Lens to Focal Plane

Now complex amplitude distribution in the exit plane of the lens is obtained. Wave propagation from the exit plane of the micro-Fresnel lens to the focal plane is treated with the concept of propagation of the angular spectrum [12].

At first, the complex amplitudes are Fourier transformed to yield the angular spectrum at $z = 0$,

$$A_j(0) = \text{DFT}\{u(n,0)\}. \tag{10}$$

Here, DFT denotes discrete Fourier transform and in practice it is computed with a FFT algorithm. The angular spectrum in the plane at a distance z away from the exit plane of the micro-Fresnel lens is given by

$$A_j(z) = A_j(0)\exp[i(2\pi n_2/\lambda)z\sqrt{1 - (\nu_j\lambda/n_2)^2}], \tag{11}$$

where $\nu_j = j/2r$ is the spatial frequency of a plane wave propagating in the direction of $\sin^{-1}(\nu_j\lambda/n_2)$. Then, the complex amplitude of the same plane is obtained as

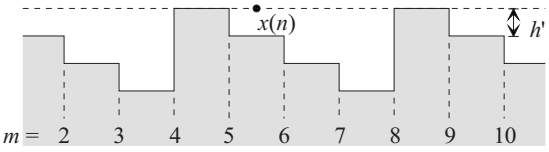

Fig. 3. Sampling point and grating depth in the case of $L = 4$, as an example.

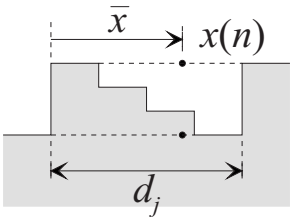

Fig. 4. Definition of local period and application of the FMM.

$$u(n,z) = \mathrm{IDFT}\{A_j(z)\}, \tag{12}$$

where IDFT denotes inverse discrete Fourier transform, and the finally observed value is the intensity profile

$$I(n) = |u(n,z)|^2. \tag{13}$$

One of the advantages of using angular spectrum representation is that the effect of defocusing can be easily computed with Eq. (11).

3. RESULTS

We present results of numerical simulation of focusing properties of normally illuminated one-dimensional micro-Fresnel lenses with LGT. To evaluate reliability of the LGT, obtained results are compared with two well-established fully electromagnetic numerical methods, i.e., the FMM and FDTD methods together with experimental observation. In the present analysis, the propagation process from Eq. (10) to Eq. (13) is the same for all three methods. The parameters of the three lenses considered here are given in Table 1.

As described in Section 2, the straightforward implementation of the LGT assumes illumination of an optical element, i.e., a micro-Fresnel lens here, by a plane wave. This is tricky and contradictory, because a plane wave assumes an infinitely wide space, strictly speaking. So, the actual model here is that at each sampling point a light wave with unit amplitude is normally incident on the lens. This model considers the cylindrical micro-Fresnel lens as an infinite lens array with both the FMM and the FDTD methods, in which an individual micro-Fresnel lens corresponds to a grating period. As the output wave from the lens is focused, any effect of the diffracted wave from neighboring periods would be negligible at least near the focal spot, and thus treating a single lens as a lens array would not be unrealistic. This view is also supported by a remark in the Discussion and Conclusions of [7].

As to experiments, focused spot profiles were measured by the setup shown in Fig. 5. Introduction of a quarter-wave plate and a polarizer in the setup was for changing the polarization state of the incident wave easily. Figure 6 shows a central 275 μm$\times$210 μm portion of a micro-Fresnel lens of $f=1$ mm and $r=0.75$ mm fabricated on a silica substrate by electron-beam lithography. Careful examination of this micrograph reveals that the widths of ridges were 0.1 μm greater than designed values over the entire area of the lens, while sizes of local periods were correctly realized. This fact was reflected in the following simulation for Cases B and C.

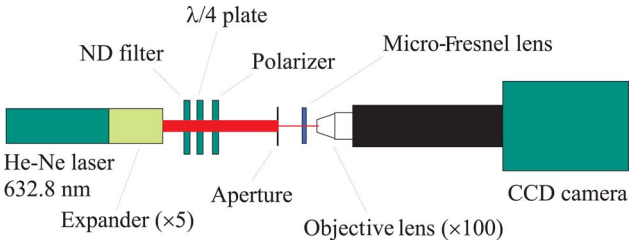

Fig. 5. (Color online) Experimental setup.

Parameters used in the simulation are listed in Table 2. These values should be accepted as a set of necessary conditions for accurate computation considering convergence; justification for this is explained below in Section 4.

A. Case A

Case A is a four-phase-level lens of $f=100\lambda$ and $r=50\lambda$, thus giving $f/1$, as an object of numerical simulation only. The number of sampling points N for the FDTD method is four times the value of the other methods, because a cell size of $\approx\lambda/40$ corresponding to $N=4096$ is required to conduct accurate computation.

Intensity profiles of a focused spot in the best focal planes are shown in Fig. 7(a). Here, vertical scale is normalized with intensity of the incident wave, i.e., correctly including the effects of reflection and diffraction. It can be observed that the curves for the LGT, FMM, and FDTD methods are almost the same, but the best focal planes are at different axial positions between 0.5λ and 0.7λ as given in the caption of Fig. 7. Also included in the figure denoted as "ideal" (top curve) is a result assuming an idealized aberration-free lens just as a reference. In this case, the vertical scale is determined by multiplying $I(n)$ in Eq. (13) by $(1-R)\mathrm{sinc}(1/L)$, R being Fresnel reflection, in order to include the effects of reflection and diffraction.

Shown in Fig. 7(b) is the change of intensities on the axis, i.e., the effects of defocusing. Although there are some differences in detail shape of the curves among the three methods, overall tendency is again almost the same, in particular near the best focal position. Deviation from a

Table 1. Parameters of Simulated Lenses

Case	f	r	L	No. of Zones	Zone Width (Max)	Zone Width (Min)
A	100λ	50λ	4	12	14.2λ	2.26λ
B	1580λ	1185λ	2	391	56.6λ	1.68λ
C	1580λ	316λ	2	60	56.6λ	5.28λ
B[a]	1 mm	0.75 mm	2	391	35.8 μm	1.06 μm
C[a]	1 mm	0.20 mm	2	60	35.8 μm	3.34 μm

[a]When $\lambda=632.8$ nm is assumed in experiments.

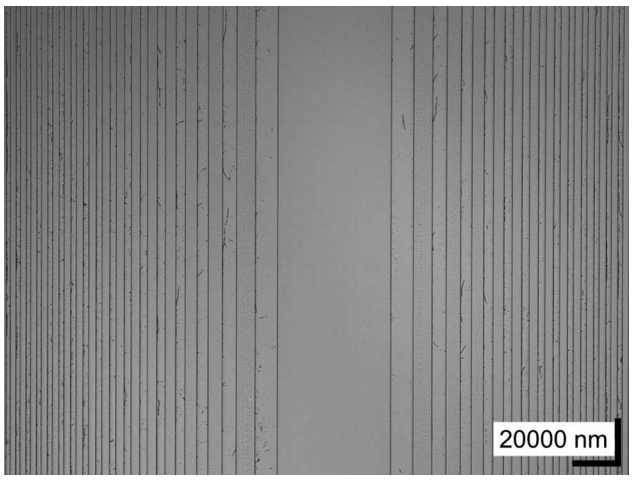

Fig. 6. Observed binary micro-Fresnel lens of $f=1$ mm.

smooth curve for the ideal lens indicates the effects of diffraction owing to the fine structure of the micro-Fresnel lens.

B. Case B

Case B is a binary-phase level lens of $f=1$ mm and $r=0.75$ mm, thus yielding $f/0.67$ designed at $\lambda=632.8$ nm. As the full aperture exceeds 1000λ, it is not possible to execute the numerical calculations with the FMM under the authors' computational environment. The results obtained with the LGT and the FDTD methods are compared with experimental data that are normalized with an axial value of the LGT, because it was difficult to measure absolute values in the experiment owing to the size of the micro-Fresnel lens.

In Fig. 8(a), we find that focused beam profiles of the LGT and FDTD methods overlap perfectly. In addition, the experimental result is almost the same, except that one of two sidelobes for the experimental result is missing. The most probable reason for the differences from the simulated results would be off-axis illumination during the measurement.

Another noticeable phenomenon is that the maximum intensities according to numerical simulation are significantly lower than for an ideal lens. The main reason for this is that first-order diffraction efficiency decreases as the grating period becomes short, in particular at around a few wavelengths; such an area occupies more than half the aperture of this lens. The phenomenon is well known and for more detail see, e.g., Fig. 4 in [7]. Despite this phenomenon, quality of the focused beam is maintained, because the FWHM for the LGT and an ideal lens are similar with values of 0.43 and 0.45 μm, respectively. In addition, good agreement among the data on the effects of axial defocusing is observed in Fig. 8(b).

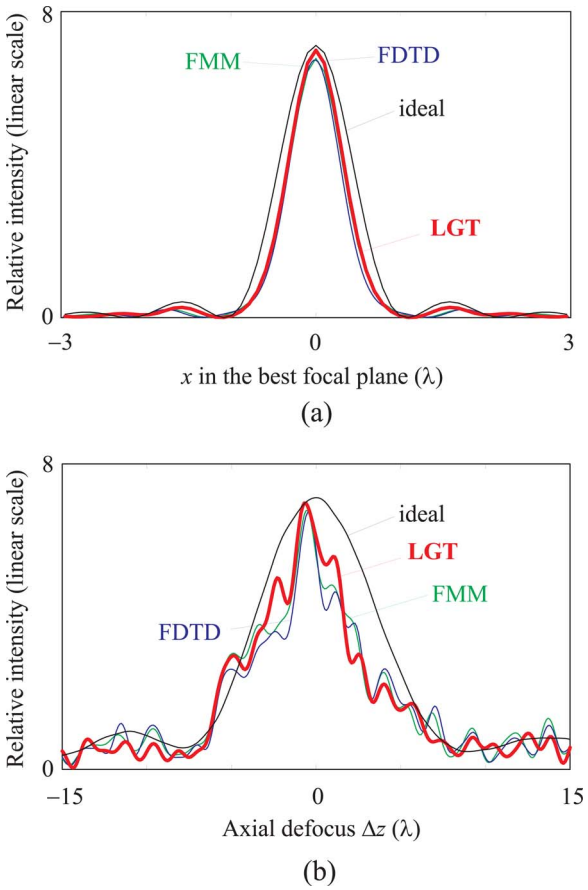

Fig. 7. (Color online) Focusing properties of a micro-Fresnel lens of $f=100\lambda$ and $r=50.4\lambda$. (a) Spot profiles: $\Delta z=-0.7\lambda$ for LGT, -0.6λ for FMM, and -0.5λ for FDTD. (b) Intensity with axial defocus.

In considering the fact that the modal method on which the LGT is based and the basis of the FDTD method are totally different numerical method techniques in principle, it must be considered impressive that the LGT and the FDTD methods gave almost the same results in Fig. 8. This would indicate the great validity and real usefulness of the LGT.

C. Case C

Case C is the same as Case B, but the aperture is restricted to $r=0.2$ mm, thus giving $f/2.5$. Here in Fig. 9, the general tendency is the same for the three curves. The somewhat deformed focused beam profiles for the LGT and FDTD method are for a defocus distance of +4.6 μm. The origin of this deformation would be explained in the

Table 2. Parameters for Simulation

Case	N	J	J_{FMM}	N_{FDTD}	Time Steps per Time Period in FDTD
A	1024	40	320	4096	64
B	32 768	40	—	131 072	128
C	8192	40	—	16 384	64

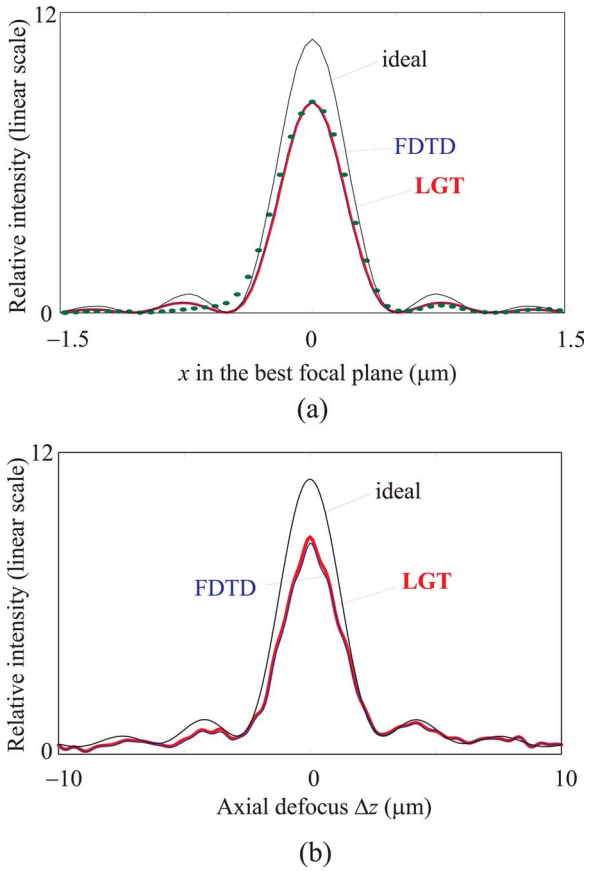

Fig. 8. (Color online) Focusing properties of a micro-Fresnel lens of $f=1$ mm and $r=0.75$ mm. (a) Spot profiles: $\Delta z=0$ for both LGT and FDTD. (b) Intensity with axial defocus.

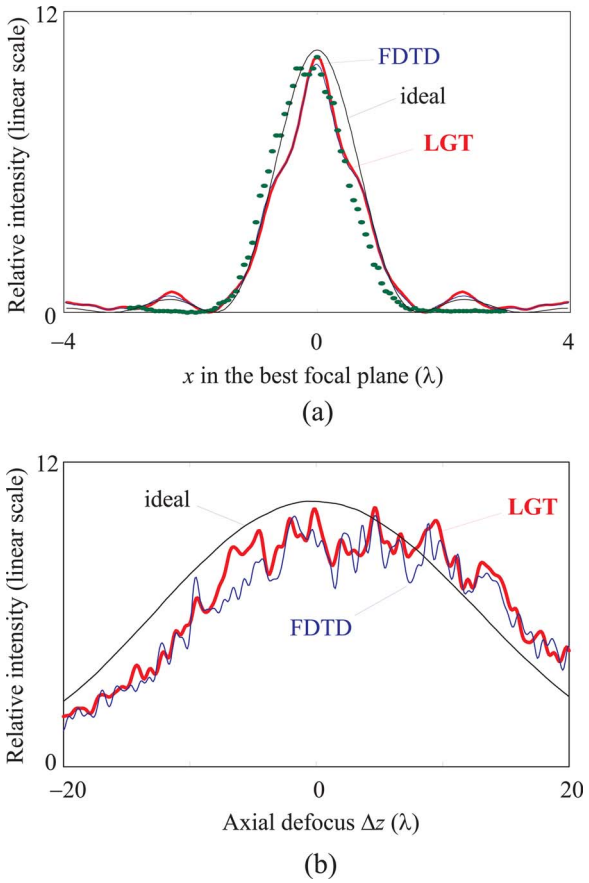

Fig. 9. (Color online) Focusing properties of a micro-Fresnel lens of $f=1$ mm and $r=0.2$ mm. (a) Spot profiles: $\Delta z=4.6$ μm for both LGT and FDTD. (b) Intensity with axial defocus.

following way. In a system of higher f number such as the Case C, higher-frequency components from neighboring periods more easily interfere with the focused beam than in a lower-f-number system such as in Case B. Obviously, a different shape of focused beam profile is obtained at a different defocus value.

Another feature in this case is that the absolute values obtained for the LGT and for the FDTD method are comparable to that of an ideal lens. The minimum zone width at the edge of this lens is 5.28λ, which is large enough to avoid the efficiency-spoiling effect for gratings in the resonance domain mentioned in Subsection. 3.B.

D. Polarization Sensitivity

The biggest reason for employing the one-dimensional micro-Fresnel lens here, while there are earlier reports [8,9] of two-dimensional analysis, is that we would like to compare the polarization properties of simulated and experimental results. In practice, we compared the power ratio within the main lobe of the focused spots to various aperture sizes as shown in Fig. 10. In the LGT, the value is estimated as the sum of $I(n)$ defined in Eq. (13) within the main lobe, while in experiments the value is the integral intensity of a CCD sensor array. Because of difficulty in accurately measuring incident power in experiments, both simulated and experimental values are normalized with the value of TM polarization at $r=0.75$ mm in Fig. 10 for easy comparison.

It is clearly seen that the focused power difference between TE and TM polarization becomes larger as the lens aperture widens. Moreover, the simulation gives quantitatively similar results to those of the experiments for wider apertures. The discrepancy for narrower apertures would be mainly due to difficulty in positioning apertures in experiments.

4. CONVERGENCE

Prior to the actual simulation in Section 3, we conducted a convergence study of each method by changing the num-

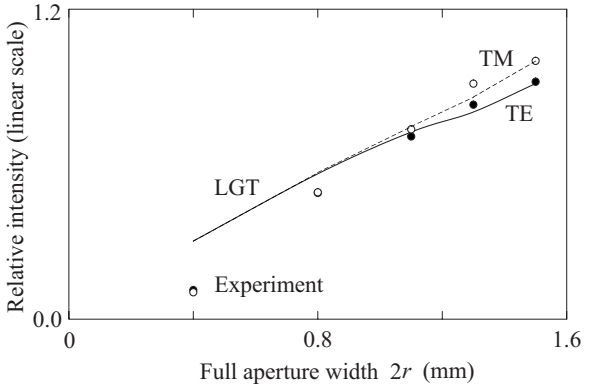

Fig. 10. Comparison between LGT and experiments: power within focused spot of a micro-Fresnel lens of $f=1$ mm. Solid curve, LGT for TE; dashed curve, LGT for TM. Solid circles, experiments for TE. Open circles, experiments for TM. All data are normalized with the value of $r=0.75$ mm for TM.

bers of truncation orders J for the LGT and FMM and unit cell sizes for the FDTD method. For this purpose, we chose Case A as a model structure.

For the LGT and FMM, the most important parameter is the number of truncation orders J, as it determines the eventual accuracy in modal methods. We first looked at the shapes of focused profile at the best focus. As they are almost independent of J, the peak intensities at $x=0$ are compared. Figure 11(a) may indicate that $J=20$ for the LGT and $J=160$ for the FMM are minimum requirements. Then, we investigated defocusing effects in Fig. 11(b), which suggests that $J=40$ for the LGT and $J=320$ for the FMM are necessary for sufficient convergence. We confirmed that a curve with $J=80$ completely overlapped with that of $J=40$ for the LGT.

While the number of sampling points N is mere spatial resolution and has no effect on quality of simulation for the LGT and FMM, it is a crucial parameter for the FDTD method. Here, we used almost the same cell size $\sim 2r/N$ for both the x and the z directions. We found that the cell size of $\lambda/40$ is necessary for accurate computation, and time steps corresponding to 30 time periods are necessary for stable computation.

For Case B, the above results are modified considering the structural differences. $J=40$ is chosen by comparing minimum feature sizes and the numbers of layers L. N and N_{FDTD} are determined by comparing lens apertures. The parameters for Case C are the same as for Case B, because it simulates simply covering the outer portion of the aperture of the lens. This is necessary for comparison with the experimental data.

It would obviously be more efficient to modify convergence conditions depending on the local period size, if an object of numerical analysis is fixed. However, our intention is applying the LGT to optimizing structure of DOEs, and in the course of the procedure, the local period size is always changing. Therefore, we decided to fix the value of J in the whole aperture.

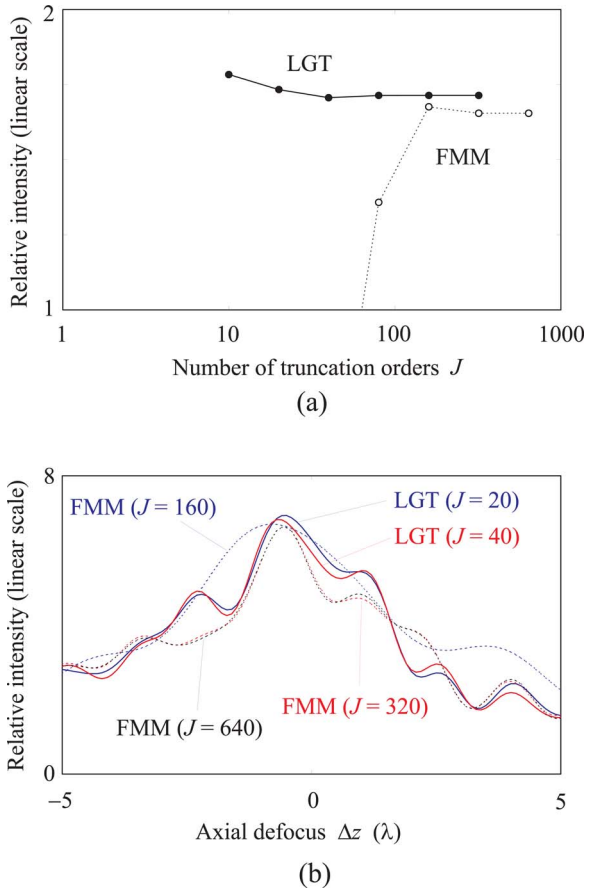

Fig. 11. (Color online) Convergence study. (a) Peak intensities at $x=0$ for the best focus. (b) Intensities at $x=0$ with axial defocus for various numbers of truncation orders.

5. DISCUSSION

We have demonstrated that the LGT does work satisfactorily with much fewer number of truncation orders than the full vectorial FMM. To explain the reason for this, let us look at the properties of local gratings over an entire lens aperture, assuming Case B as an example. In Fig. 12(a), the distribution of the local period is drawn with a solid black curve. At five selected positions, the required numbers of truncation orders for convergence of transmitted first-order diffraction efficiencies within 10^{-2}, 10^{-3}, and 10^{-4} are plotted with filled circles. Also, how this parameter converges at each position is shown in Fig. 12(b).

Obviously, the central portion of a lens is composed of local gratings of large periods that need large number of

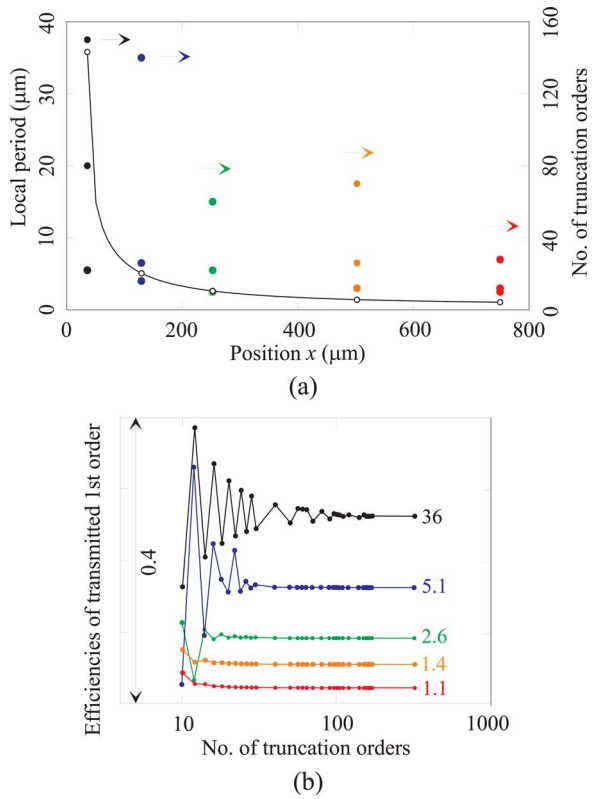

Fig. 12. (Color online) Why does the LGT work satisfactorily with a much smaller number of truncation orders than the full vectorial FMM? Case B is assumed as a model. (a) Left vertical axis, local periods of a lens; right vertical axis, required numbers of truncation orders. Three circles correspond to convergence of first-order diffraction efficiency within 10^{-2}, 10^{-3}, and 10^{-4} assuming a rectangular grating of fill factor 0.5 with the same period. (b) Convergence of transmitted first order for the grating mentioned in (a). The values denote the grating period in μm.

truncation orders, but this area is limited. For example, at $x=129$ μm the local period is 5.1 μm, and only 26 truncation orders ensure convergence within 10^{-3}. This means that 83% of the lens aperture can be handled with fewer truncation orders. Therefore, the LGT would give comparable results with much fewer number of truncation orders than the case in which the entire aperture is considered as a grating period.

The fewer number of truncation orders means faster computation. Relative computation time for the LGT and FMM assuming Case A is shown in Fig. 13. For the same J, the LGT needs more time than the FMM, because it has to conduct the process of the FMM for each local grating structure. However, as described in Section 4, the LGT needs only $J=40$ for computation of the same accuracy as the FMM with $J=320$. As a result, the LGT is 77 times faster than the FMM for this particular problem. This is shown in Table 3, which summarizes relative computation time considering convergence.

In comparing with the FDTD method, the advantage of the LGT is more notable, because the FDTD method needs finer sampling point spacing for computation of the same accuracy. This is particularly important in computing large structures such as in Case B.

6. CONCLUSION

We have demonstrated enormous potential and usefulness of the LGT, that is, treating local structures of optical elements larger than the wavelength as diffraction gratings. The method is based on the FMM, but needs many fewer truncation orders than the direct application of the FMM, which treats the diffractive lens as a whole. Its biggest advantage is computation speed: tens to thousands times faster, depending on problems treated, than straightforward implementation of existing numerical methods to obtain results with similar accuracy.

Another advantage of the concept of the LGT is that any rigorous grating electromagnetic method e.g., C [13], differential [14], integral [15], boundary integral [16], and finite element [17] methods, can be used by simply replacing the FMM here with them.

Although rigorously speaking the LGT may not be a genuine electromagnetic numerical method, it can provide comparable results as shown here, and there are numerous applications that would benefit from the LGT in practical optical design communities.

We believe that the real potential of the LGT is in analysis of two-dimensional optical elements and are at the moment working on its formulation together with experimental verification.

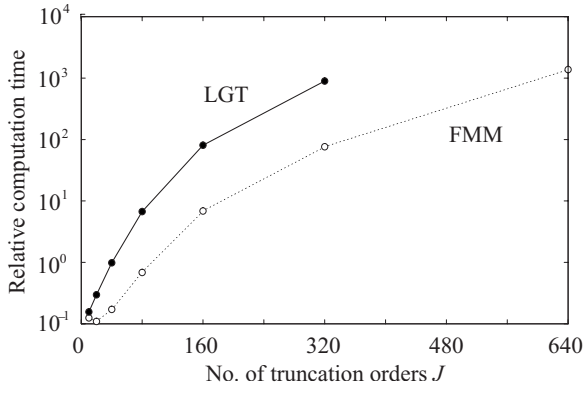

Fig. 13. Comparison of computation time between the LGT and FMM with various numbers of truncation orders.

Table 3. Relative Computation Time for the Same Quality of Computation

Case	LGT	FMM	FDTD
A	1	77	240
B	1	—	1900
C	1	—	580

REFERENCES

1. J. Turunen and F. Wyrowski, "Introduction to diffractive optics," in *Diffractive Optics for Industrial and Commercial Applications*, J. Turunen and F. Wyrowski, eds. (Akademic Verlag, 1997), pp. 11–12.
2. M. Lang and T. D. Milster, "Investigation of optics in the 10–200 μm regime," Opt. Rev. **14**, 189–193 (2007).
3. D. W. Prather, S. Shi, and J. S. Bergey, "Field stitching algorithm for the analysis of electrically large diffractive optical elements," Opt. Lett. **24**, 273–275 (1999).
4. A. v. Pfeil, F. Wyrowski, A. Drauschke, and H. Aagedal, "Analysis of optical elements with the local plane-interface approximation," Appl. Opt. **39**, 3304–3313 (1999).
5. T. Vallius, M. Kuittinen, J. Turunen, and Ville Kettunen, "Step-transition perturbation approach for pixel-structured nonparaxial diffractive elements," J. Opt. Soc. Am. A **19**, 1129–1135 (2002).
6. G. H. Spencer and M. V. R. K. Murty, "General ray-tracing procedure," J. Opt. Soc. Am. **52**, 672–678 (1962).
7. E. Noponen, J. Turunen, and A. Vasara, "Electromagnetic theory and design of diffractive-lens arrays," J. Opt. Soc. Am. A **10**, 434–443 (1993).
8. Y. Sheng, D. Feng, and S. Larochelle, "Analysis and synthesis of circular diffractive lens with local linear grating model and rigorous coupled-wave theory," J. Opt. Soc. Am. A **14**, 1562–1568 (1997).
9. B. H. Kleemann and R. Güther, "Zonal diffraction efficiencies and imaging of micro-Fresnel lenses," J. Mod. Opt. **45**, 1405–1420 (1998).
10. J. Turunen, "Diffraction theory of microrelief gratings," in *Micro-Optics*, H. P. Herzig, ed. (Taylor & Francis, 1997), pp. 31–52.
11. A. Taflove and S. C. Hagness, *Computational Electrodynamics: the Finite-Difference Time-Domain Method* (Artech House, 2000).
12. J. W. Goodman, *Introduction to Fourier Optics* (McGraw-Hill, 1996), pp. 55–61.
13. L. Li, J. Chandezon, G. Granet, and J.-P. Plumey, "Rigorous and efficient grating-analysis method made easy for optical engineers," Appl. Opt. **38**, 304–313 (1999).
14. F. Montiel and M. Nevière, "Differential theory of gratings: extension to deep gratings of arbitrary profile and permittivity through the R-matrix propagation algorithm," J. Opt. Soc. Am. A **11**, 3241–3250 (1994).
15. B. H. Kleemann, A. Mitreiter, and F. Wyrowski, "Integral equation method with parametrization of grating profile theory and experiments," J. Mod. Opt. **43**, 1323–1349 (1996).
16. D. W. Prather, M. S. Mirotznik, and J. N. Mait, "Boundary integral methods applied to the analysis of diffractive optical elements," J. Opt. Soc. Am. A **14**, 34–43 (1997).
17. G. Bao, Z. Chen, and H. Wu, "Adaptive finite-element method for diffraction gratings," J. Opt. Soc. Am. A **22**, 1106–1114 (2005).